ACS OMEGA

http://pubs.acs.org/journal/acsodf

Article

Anode Properties of $Cr_xV_{1-x}Si_2$/Si Composite Electrodes for Lithium-Ion Batteries

Yuta Kimura, Yasuhiro Domi, Hiroyuki Usui, and Hiroki Sakaguchi*

Cite This: *ACS Omega* 2021, 6, 8862−8869

Read Online

ACCESS | Metrics & More | Article Recommendations | Supporting Information

ABSTRACT: We have reported the effects of substituting a transition metal in silicide on the electrochemical performance of the silicide/Si composite anode for lithium-ion batteries (LIBs); the $Cr_{0.5}V_{0.5}Si_2$/Si electrode exhibited much better cyclability compared with $CrSi_2$/Si and VSi_2/Si electrodes. Herein, we investigated the electrochemical performance of a $Cr_xV_{1-x}Si_2$/Si slurry electrode for its application in LIBs, and the results obtained were compared to those of a gas deposition (GD) electrode, which was comprised of only active materials. The slurry electrode exhibited a superior cycling life as with the GD electrode. After charge−discharge cycles, the expansion of the electrode thickness of $CrSi_2$/Si and $Cr_{0.5}V_{0.5}Si_2$/Si was smaller than that of VSi_2/Si, and VSi_2 was significantly pulverized compared with the other silicides. It is considered that VSi_2 deformed easily by the stress from Si expansion and pulverized because the hardness of VSi_2 was the smallest among the silicides used in this study. These results reveal that $Cr_{0.5}V_{0.5}Si_2$/Si has great potential as an anode material for next-generation LIBs and hardness is an important property for compositing silicide with Si.

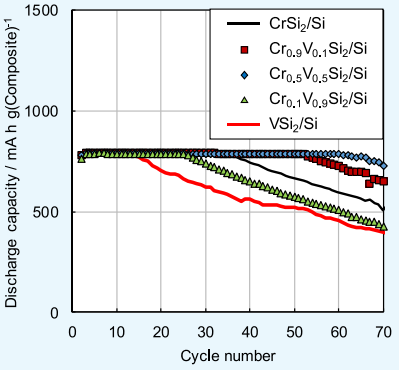

INTRODUCTION

The popularization of electric vehicles has resulted from the need to prevent global warming, and lithium-ion batteries (LIBs) are used in the power supplies of electric vehicles. The increase in the energy density of LIBs is highly desirable because the cruising distance of conventional electric vehicles is only approximately 400 km.[1−3] Graphite is employed as an anode active material in LIBs; its effective capacity is approximately equal to its theoretical capacity (372 mA h g^{-1}), so any further improvement with respect to its capacity is difficult. Therefore, Si, having a theoretical capacity 10 times that of graphite (3580 mA h g^{-1}), is used instead. However, Si facilitates the formation of a $Li_{15}Si_4$ phase, where Si absorbs Li to a large extent at room temperature, expanding by approximately 3.8 times.[4] Because of the repeated charging and discharging, Si exhibits poor cyclability because Si pulverizes owing to the accumulation of strains, resulting from the change in volume.

In order to improve the cyclability of Si, alloying Si with metal elements such as Cu or Ni has been addressed.[5−8] We have confirmed that the cyclability can be improved by compositing transition metal silicide with Si (silicide/Si). We have also reported that the materials to be composited with Si require the following four properties:[9−20]

(1) Mechanical properties suitable for the relaxation of the stress from Si
(2) High electronic conductivity
(3) Moderate reactivity with Li^+
(4) High thermodynamic stability

Optimizing all the four properties together is difficult in binary silicides. Hence, we have tried to improve the properties of silicides and the anode performance of composite electrodes for LIBs by compositing ternary silicides. As a result, we have found that ternary $LaNi_xSi_{2-x}$ (AB_xSi_{y-x}-type, A and B:metal), where Ni partially replaces Si in $LaSi_2$, can be synthesized and the $LaNi_{0.1}Si_{1.9}$/Si electrode exhibits improved cycling and high-rate performances compared with the $LaSi_2$/Si electrode.[21] Furthermore, we have observed that a part of Cr is replaced by V, forming $Cr_xV_{1-x}Si_2$ ($A_{1-x}B_xSi_y$-type), when V is added to $CrSi_2$. The $Cr_{0.5}V_{0.5}Si_2$/Si electrode exhibited significantly better cycling stability than the $CrSi_2$/Si or VSi_2/Si electrode.[22]

We have investigated the changes in the four aforementioned properties of ternary silicide. We have confirmed that property (4) is improved by replacing V, whereas properties (1) and (2) did not change. Properties (1) and (2) correspond to the parameters of the elastic modulus and electrical conductivity, respectively. Property (3) is improved because of the enlargement of the crystal lattice of ternary silicide, resulting from the substitution of Cr (atomic radius: 0.128 nm) by V (atomic radius: 0.134 nm). Furthermore, we found that

Received: December 9, 2020
Accepted: February 26, 2021
Published: March 26, 2021

https://doi.org/10.1021/acsomega.0c05986
ACS Omega 2021, 6, 8862−8869

the charge repulsion between Li and the transition metal in $CrSi_2$ is smaller than the charge repulsion between Li and VSi_2, based on the results of a first-principles calculation. From the above results, it may be considered that the Li diffusion in $Cr_{0.5}V_{0.5}Si_2$ is facilitated by the following two factors: a large crystal lattice of VSi_2 and a small charge repulsion between Si and $CrSi_2$. As a result, the stress generated during the charge reaction is homogenized by the smooth diffusion of Li into the Si phase through the silicide phase, followed by the absorption of Li in the Si phase homogeneously. Consequently, we concluded that the ternary silicide/Si composite exhibited better cycling stability than the binary silicide/Si composite, based on the aforementioned results.

The above results were obtained using a gas deposition electrode, composed of only an active material. In this study, we evaluated the LIB anode performance of $Cr_xV_{1-x}Si_2$/Si using a slurry electrode consisting of an active material, a conductive agent, and a binder, in order to check its potential for application as an anode material of LIBs. We also investigtaed the change in the metallographic structure of $Cr_xV_{1-x}Si_2$/Si following the charge−discharge cycles to clarify the mechanism of capacity reduction.

RESULTS AND DISCUSSION

Characterization. Figure 1 shows the X-ray diffraction (XRD) patterns of the powders prepared from Cr, V, and Si. Additionally, Table 1 summarizes the corresponding lattice parameters. The $CrSi_2$/Si binary phase was confirmed from the Si and $CrSi_2$ peaks. All peaks of VSi_2/Si were also assigned to Si and VSi_2. The ternary composites were confirmed from the presence of Si peaks, similar to the binary silicide/Si composites (Figure 1a). The silicide peaks of $CrSi_2$ shifted to lower angular values with the increase in the amount of V (Figure 1b). In addition, the lattice constant along the *a*-axis increased (Table 1). These results indicate that some of the Cr atoms in $CrSi_2$ are substituted by V, where the radius of V is larger than that of Cr. Thus, we confirmed that the ternary silicide/Si composites prepared in this study were composed of Si and $Cr_{1-x}V_xSi_2$, as intended.

The field-emission electron probe microanalysis (FE-EPMA) results for $Cr_{0.1}V_{0.9}Si_2$/Si are shown in Figure 2. The white area of the scanning electron microscopy (SEM) image (Figure 2a) indicates Si, Cr, and V, and the concentrations of Cr and V in the white area were higher than those in the black area (Figure 2c,d). In contrast, the black area mainly consisted of Si (Figure 2b). These results support the conclusion that the white area is the silicide phase and the black area is the Si phase, as shown in Figure 2a. Figure 3 shows the cross-sectional SEM images of a composite ribbon. The structure of the prepared composites showed that the silicide phases were surrounded by the Si phases. Additionally, there were no significant differences in the shape and size of the silicide phase in any composite. Despite the variation in the composition, the composite had similar structures. In addition, Figure 2a shows that the Si phases and silicide phases are finely gathered together in the gray area. In addition, the entire cross-sectional SEM images of composite ribbons are shown in Figure 4. When alloy ribbons are prepared by roll quenching, the structure of the side touched with the roll during quenching (roll side) is easier to become fine than that of the opposite side (free side) because the cooling speed of the roll side is faster than the free side.[25,26] However, we could confirm no difference in the structure of the silicide/Si composite ribbons prepared in this study on each side. Figure S1 shows the schematic diagram of the roll-quenching method and the relationship between the roll side and the free side as a reference.

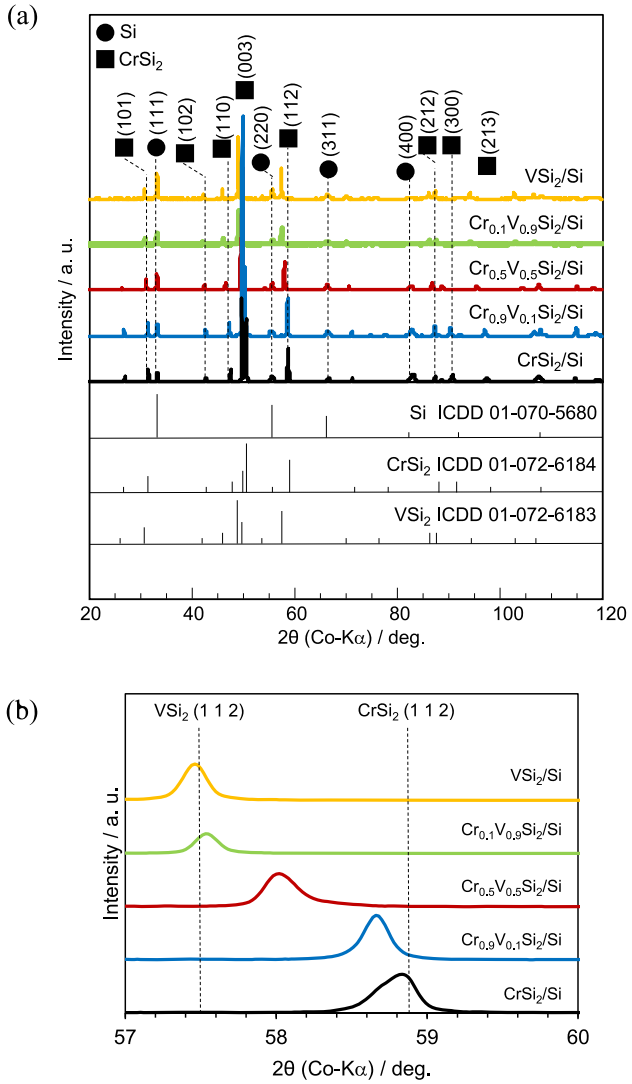

Figure 1. (a) XRD patterns of the synthesized silicide/Si composites and (b) their enlarged view between 57 and 60°.

Table 1. Lattice Constant of the Silicide Phase in Each Silicide/Si Composite

		lattice constant of silicide (Å)	
sample	crystal structure of silicide	a axis	c axis
$CrSi_2$/Si	hexagonal	4.435	6.377
$Cr_{0.9}V_{0.1}Si_2$/Si		4.458	6.366
$Cr_{0.5}V_{0.5}Si_2$/Si		4.504	6.404
$Cr_{0.1}V_{0.9}Si_2$/Si		4.572	6.380
VSi_2/Si		4.579	6.384

Charge−Discharge Cycling Test of the Silicide/Si Composite Electrodes. Figure 5 shows the initial charge−discharge curves of each silicide/Si composite electrode. For the all electrodes, potential plateaus appeared for the charge (lithiation) reaction at around 0.1 V vs Li/Li^+ and for the discharge (delithiation) reaction at approximately 0.45 V vs Li/Li^+. The plateaus are attributed to the alloying and

https://doi.org/10.1021/acsomega.0c05986
ACS Omega 2021, 6, 8862−8869

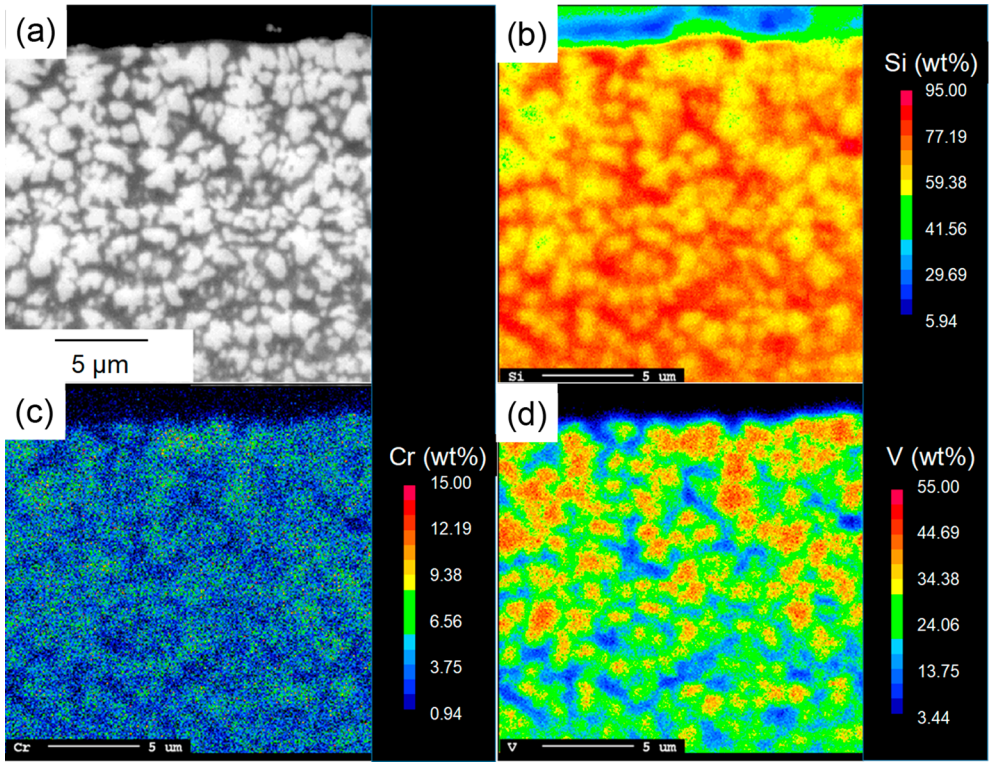

Figure 2. (a) SEM image of $Cr_{0.1}V_{0.9}/Si$ and the corresponding FE-EPMA maps of (b) Si, (c) Cr, and (d) V. The scale bar denotes 5 μm.

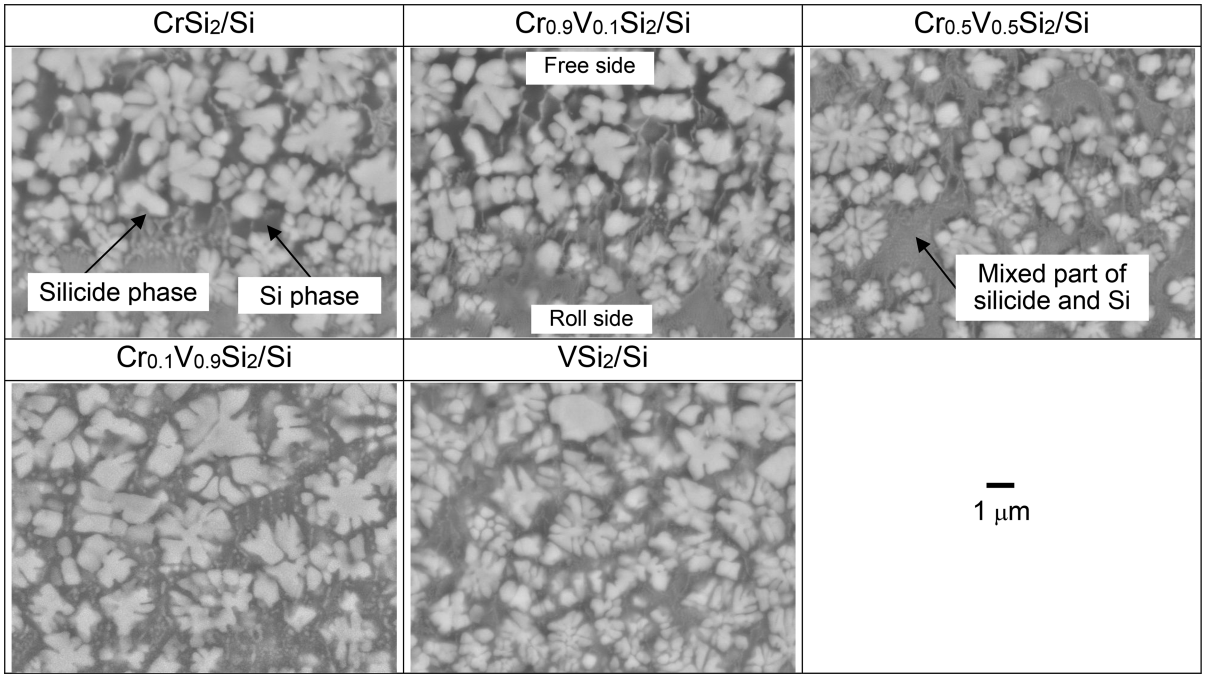

Figure 3. Cross-sectional SEM images of the prepared composites. The scale bar denotes 1 μm.

dealloying reactions of Si and Li. We considered that the silicide phase in the silicide/Si composite electrodes did not react with the Li-ion because we have confirmed that only lithiation of Si in the $FeSi_2$/Si electrode should occur while both $FeSi_2$- and Si-alone electrodes reacted with Li.[27]

The initial charge and discharge capacity of the electrodes were almost the same. Additionally, there is little difference in the initial charge−discharge behavior among each silicide/Si composite electrode. Figure 6 shows the cycling life of each silicide/Si composite electrode with a charge capacity limit of 800 mA h g (silicide/Si composite)$^{-1}$. In addition, Coulombic efficiency is also shown in Figure 7. The $Cr_{0.9}V_{0.1}Si_2$/Si and $Cr_{0.5}V_{0.5}Si_2$/Si composite electrodes exhibited better cycling stabilities compared with $CrSi_2$/Si, owing to the addition of V. In particular $Cr_{0.5}V_{0.5}Si_2$/Si exhibited the best cycling stability. However, because of the increased amount of V in $Cr_{0.1}V_{0.9}Si_2$/Si and VSi_2/Si electrodes, they exhibited poor cycling stabilities and their Coulombic efficiencies were decreased from the

https://doi.org/10.1021/acsomega.0c05986
ACS Omega 2021, 6, 8862−8869

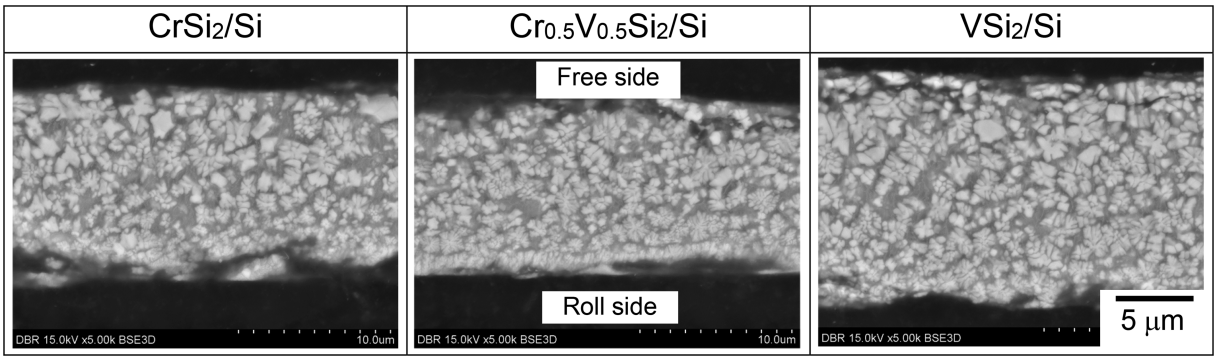

Figure 4. Entire cross-sectional SEM images of the prepared composites. The scale bar denotes 5 μm.

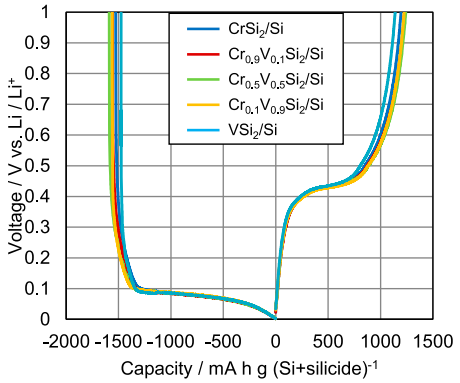

Figure 5. Initial charge−discharge curve of various silicide/Si composite electrodes in 1 M $LiPF_6$ in EC + DEC (EC/DEC = 1:1 vol %).

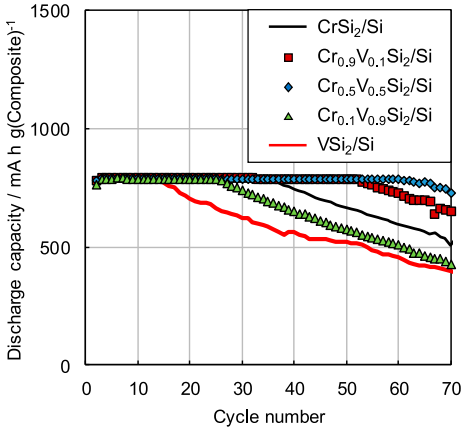

Figure 6. Cycle life of various silicide/Si composite electrodes in 1 M $LiPF_6$ EC/DEC (EC/DEC = 1:1 vol %).

beginning of the cycle. It is considered that the decrease in the Coulombic efficiency is caused by surface film formation on the new Si surface created by particle pulverization. We confirmed that $Cr_{0.5}V_{0.5}Si_2$/Si can be applied as a composite electrode in practical applications because it exhibited the best cycling performance as with the gas deposition (GD) electrodes.

Cross-Sectional Observation of Electrodes after Charge−Discharge. Figure 8 shows the cross-sectional SEM images of $CrSi_2$/Si, $Cr_{0.5}V_{0.5}$/Si, and VSi_2/Si electrodes before and after the 50th charge−discharge cycle. The highly magnified SEM images of the composite electrodes are also shown in Figure 9. In Figure 8, it was clear that the composite

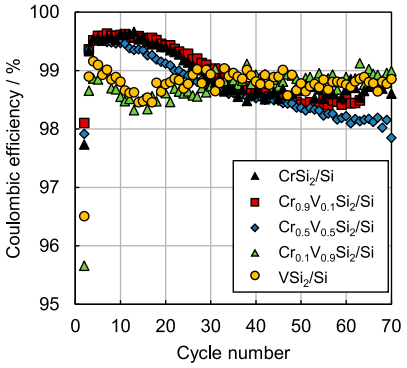

Figure 7. Coulombic efficiency of various silicide/Si composite electrodes in 1 M $LiPF_6$ EC/DEC (EC/DEC = 1:1 vol %) during the charge−discharge test.

particles existed in the electrode after the 50th cycle; exfoliation of the composite particles from the current collector was not observed in any composite electrodes. In VSi_2/Si, the thickness of the electrode doubled and large cracks occurred in the electrode after the 50th cycle. The increase in the electrode thickness of both the $CrSi_2$/Si and $Cr_{0.5}V_{0.5}$/Si composites was approximately 1.5 times in each. In Figure 9, we observed that the silicide phase was pulverized and microcracks occurred in the composite particles after the charge−discharge cycles. The calculated average diameter results of the silicide phases before and after charge−discharge are shown in Table 2. After the 50th cycle, the silicide phases of all the composites became smaller and the silicide phases of VSi_2/Si were significantly pulverized compared with those of $CrSi_2$/Si and $Cr_{0.5}V_{0.5}Si_2$/Si.

In the pulverizing silicide phase, the expansion of the composite particles becomes large owing to the cracks that occur in the particle in addition to the expansion of Li storage of the Si phase. As a result, the stress imposed on the entire electrode layer increases and the exfoliation at the interface between the active material and binder or collapse of the binder occurs. It is considered that the cycling stability of VSi_2/Si decreased because the electron conductive path or the Li-ion conductive path was lost owing to the hard pulverization of the silicide phases. The Coulombic efficiency of the VSi_2/Si electrode reduced from the initial cycle, which indicates that the pulverization occurred from the initial cycle. The volume change of silicide during charge−discharge is small compared with Si because the amount of Li-ion storage of silicide is much smaller than that of Si.[21,23,24] Therefore, it is assumed that the silicide was transformed and cracked by the stress generated during the expansion of the Si phase. We measured the

https://doi.org/10.1021/acsomega.0c05986
ACS Omega 2021, 6, 8862−8869

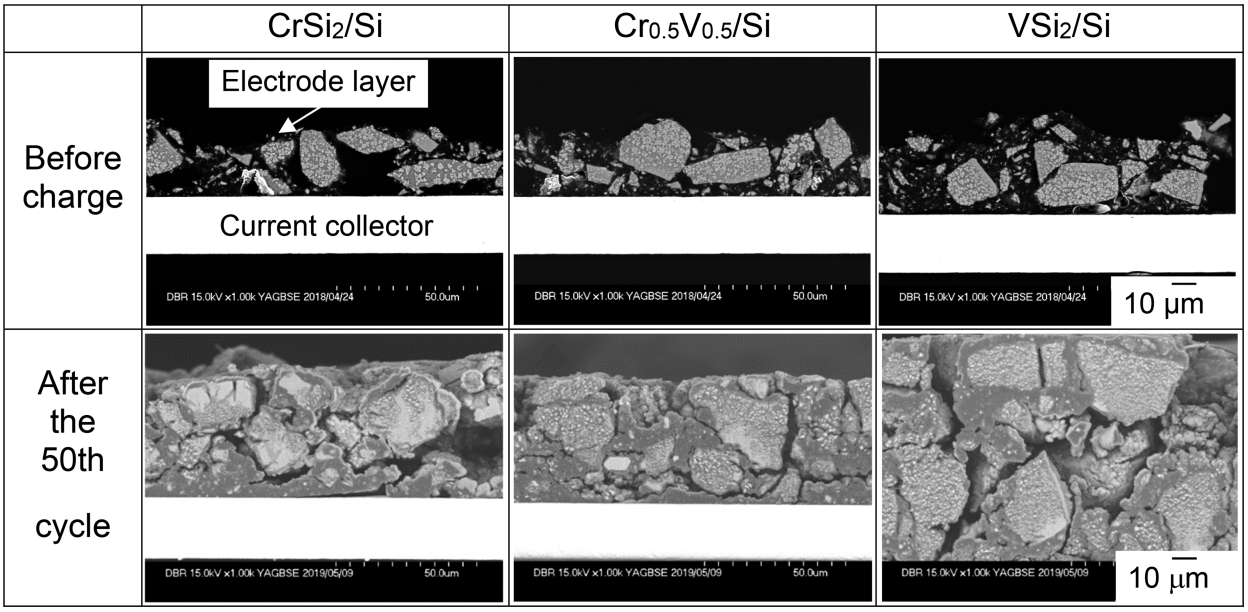

Figure 8. Cross-sectional SEM images of silicide/Si composite electrodes before and after the 50th cycle. The scale bar denotes 10 μm.

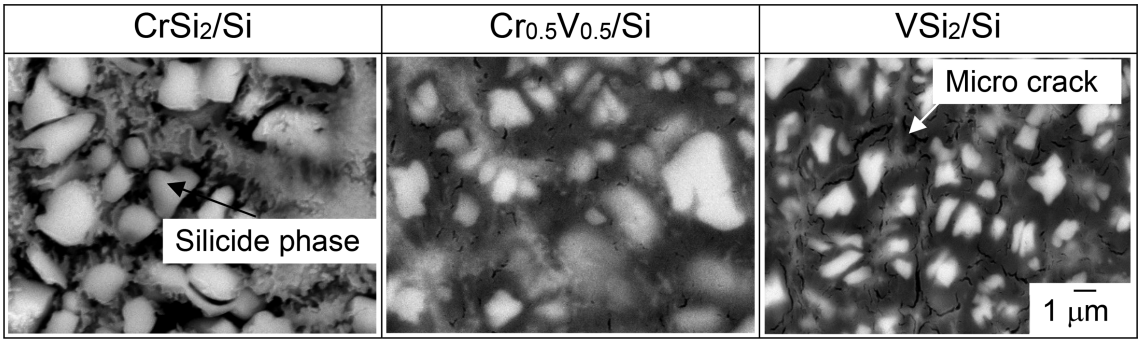

Figure 9. Cross sectional SEM images of silicide/Si composite electrodes after the 50th cycle. The scale bar denotes 1 μm.

Table 2. Calculated Average Size of the Silicide Phase before and after the 50th Cycle

	average size of silicide phase (μm)	
sample	before charge	after 50th cycle
$CrSi_2$/Si	3.0 ± 0.2	2.3 ± 0.5
$Cr_{0.5}V_{0.5}Si_2$/Si	3.2 ± 0.2	1.4 ± 0.3
VSi_2/Si	3.5 ± 0.3	0.8 ± 0.2

hardness of silicide, a parameter of deformability under the application of an external stress, to investigate the factors affecting the pulverization of the silicide phases.

Relationship between Hardness of the Silicide Phase and Cycling Stability of the Silicide/Si Composite. Figure 10 shows the correlation between the Vickers hardness of silicides and the substituent constituents of the silicide phase. $CrSi_2$ exhibited the highest resistance to pulverization after charge−discharge and was the hardest among all the evaluated silicides. In addition, the hardness of the silicide decreased as the substitution amount of V increased with the addition of V to $CrSi_2$. There is a correlation between the hardness of the silicide phase and the resistance to pulverization of silicide during charge−discharge because the silicide phase pulverizes with the increase in the substitution amount of V, as shown in Table 2. When the hardness of silicide is increased, the silicide

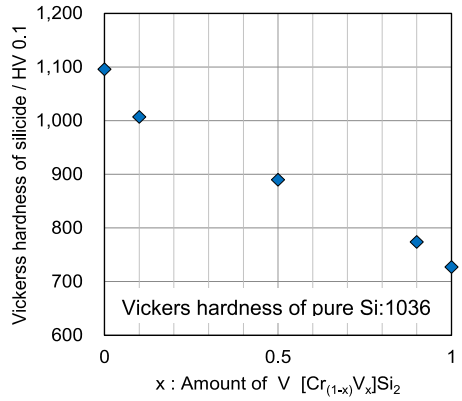

Figure 10. Correlation between Vickers hardness of silicides and x in $Cr_{1-x}V_xSi_2$.

deformation because of the stress of Si expansion becomes smaller and it becomes difficult to pulverize the silicide. Hence, it is considered that the effect of prevention of crack occurrence and shape maintenance of composite particles can become greater. Based on the above results, it is suggested that compositing a silicide with high hardness and inhibiting pulverization of silicide is effective in improving the cycling stability of silicide/Si composites.

https://doi.org/10.1021/acsomega.0c05986
ACS Omega 2021, 6, 8862−8869

In our previous studies, we have revealed that the addition of V to $CrSi_2$ improves the thermodynamic stability and spreads the crystal lattice of silicide.[21] In addition, we have found that the charge repulsion between Li and the transition metal in $CrSi_2$ is smaller than that in the case of VSi_2. We have reported that the diffusion of Li-ions in $Cr_{0.5}V_{0.5}Si_2$ was substantially improved by combining the effects of the small charge repulsion from $CrSi_2$ and the large crystal lattice of VSi_2. Besides the previous results, in this study we found that, although the hardness of $Cr_{0.5}V_{0.5}Si_2$ is smaller than that of $CrSi_2$, it is relatively high. Therefore, it is considered that it is difficult to pulverize the $Cr_{0.5}V_{0.5}Si_2$/Si composite during charge−discharge and maintain the shape of the particles. Consequently, we revealed that hardness is an important mechanical property for compositing materials with Si, in addition to the elastic modulus that has also been measured in our previous study. As shown in Figure 2 or 3, the silicide phases were surrounded by the Si phases in the silicide/Si composite particles. It is inferred that in the case of the structure above mentioned, the hardness of silicide is important because silicide is needed to not deform and maintain the shape of the composite particles during Si expansion. Conversely, when the silicide phases surround the Si phases, the silicide phases relax the stress of Si expansion, so the elastic modulus of silicide is required.

CONCLUSIONS

The electrochemical performance of the $Cr_xV_{1-x}Si_2$/Si composite electrode was evaluated. The $Cr_{0.5}V_{0.5}Si_2$/Si composite electrode exhibited the best cycling stability, similar to the GD electrode, and has great potential as an anode material for next-generation lithium ion batteries. From the results of the cross-sectional SEM observation of the composite electrode following the cycling test, it was observed that silicide pulverization and the expansion of the $CrSi_2$/Si composite electrode after charge−discharge were suppressed. This is because $CrSi_2$ is difficult to deform during Si expansion owing to the hardness. It was concluded that the $Cr_{0.5}V_{0.5}Si_2$/Si composite electrode exhibited excellent cycling stability because of the prevention of silicide pulverization in $CrSi_2$ and the improvement of Li-ion diffusion owing to the substitution of V, as previously reported. Additionally, when the structure of the silicide/Si composite is such that Si phases were surrounded by the silicide phases, the hardness of silicide is an important property for preventing the pulverization of the composite during charge−discharge.

EXPERIMENTAL SECTION

Preparation of the Silicide/Si Composite. We prepared silicide/Si composites (silicide/Si = 67:33 wt %) based on the ratio of Cr to V in the silicide phase. The constituents of each silicide/Si composite are shown in Table 3. The composite was prepared using the roll-quenching method. First, we melted Si and the additive elements (total weight = 50 g) in a button arc furnace and produced Si alloy ingots. The current value during melting was between 100 and 300 A, and the melting was conducted in an Ar atmosphere. Subsequently, the Si alloy ingot was melted at 1973 K in an induction furnace in the Ar atmosphere. A Boron nitride crucible was employed for suppressing the reaction with molten alloy. The molten alloy was dropped on a copper roll rotating at 40 m/s. Thereafter, we quenched the molten Si alloy rapidly and prepared Si alloy ribbons with a thickness of approximately 20 μm. Figure 11 shows a photograph of the Si alloy ribbon. We prepared alloy powders (active materials) by hand milling and classified them as <25 μm of alloy ribbons.

Table 3. Contents of the Synthesized Silicide/Si Composites

	Contents of the silicide/Si composite (mass %)			phase ratio (mass %)	
sample name	Si	Cr	V	silicide	Si
$CrSi_2$/Si	67.8	32.2		67	33
$Cr_{0.9}V_{0.1}Si_2$/Si	67.8	29.1	3.1		
$Cr_{0.5}V_{0.5}Si_2$/Si	68.0	16.2	15.8		
$Cr_{0.1}V_{0.9}Si_2$/Si	68.1	3.2	28.7		
VSi_2/Si	68.1		31.9		

Figure 11. Photograph of the silicide/Si composite ribbon prepared using the rapid quenching method.

The XRD (Smart Lab, Rigaku) measurements of the active materials were performed at 40 kV and 135 mA using Co Kα radiation. To observe the structure of the composite ribbons, we placed the composite ribbons in a Bakelite resin as the thickness direction of the ribbon became the embedded surface and polished mechanically. We used diamond sprays of 9, 3, and 1 μm and an alumina suspension of 100 nm as abrasives. We decreased the size of the abrasives and polished them. The cross-sectional observation of the alloy ribbon was performed using a field-emission scanning electron microscope (SU6600, Hitachi High-Technologies Corporation). The accelerating voltage was 15 kV. The element mapping images of Si and of the additive element were obtained via FE-EPMA (JXA-8500F, JEOL, Co., Ltd.). The accelerating voltage and irradiation current were fixed at 15 kV and 50 nA, respectively.

Electrochemical Characterization of the Silicide/Si Composite Electrode. The activate material (composite powder), a conductive assistant (Ketjen black, Carbon-EC600JD, LION SPECIALTY CHEMICALS CO., Ltd.), and a binder (polyamic acid, DREAMBOND, I. S. T Corporation) were mixed in the ratios of 80:5:15 (mass %). A slurry was prepared by dilution using *N*-methyl-2-pyrrolidone (FUJIFILM Wako Pure Chemical Corporation, Ltd.,). The slurry was coated on a SUS316L foil (thickness: 20 μm) using the doctor blade technique. The coating thickness was 50 μm. Followed by coating, the electrode sheet was dried at 343 K. Next, it was roll-pressed to ensure a 30 μm thickness of the active material layer. The active material mass of electrodes was about 3.5 ± 0.5 mg/cm^2. We punched the

https://doi.org/10.1021/acsomega.0c05986
ACS Omega 2021, 6, 8862−8869

electrode (diameter: 11 mm) onto the electrode sheet. The capacity of electrodes was approximately 4 mA h (capacity density: 4.2 mA h/cm^2). The electrodes were heated in a vacuum at 573 K for 1 h to imidize the binder. The electrochemical characterization was performed in a coin cell assembly (2032 type). The working electrode was a silicide/Si composite, the separator was a glass fiber filter, and the counter electrode was a Li metal (thickness: 1 mm, diameter: 12 mm). 1 M Lithium hexafluorophosphate ($LiPF_6$) dissolved in ethylene carbonate (EC)/diethyl carbonate (DEC) (EC/DEC = 1:1 vol %) (Kishida Chemical Co., Ltd.) was used as the electrolyte. The cell assembly was performed in an open dry chamber (HWR-60AR, DAIKIN INDUSTRIES Ltd.), at a dew point below −70 °C. An electrochemical measurement system (TOSCAT3100, TOYO SYSTEM Co., LTD.) was used for the galvanostatic charge−discharge test. The initial capacity of the electrodes was measured under a constant current (0.03 A g (silicide/Si composite)$^{-1}$). The cycling properties were evaluated with a charge capacity limit of 800 mA h g (silicide/Si composite)$^{-1}$ at 298 K. The current density was set to approximately 0.3 A g (silicide/Si composite)$^{-1}$, corresponding to a C-rate of 0.2 C, and the potential range was between 0.002 and 1.000 V vs Li^+/Li.

Measurement of Hardness of the Silicide Phase. We prepared an ingot in a button arc furnace and confirmed that these ingots consist of only silicide using XRD. The ingots were placed in Bakelite resin and mirror-polished via mechanical polishing. We used a micro-Vickers hardness tester (FM-800, FUTURE-TECH CORP.) to measure the hardness of each silicide phase. The measuring load was 100 g.

Calculation of the Average Diameter of the Silicide Phase. The average diameter of the silicide phase in the Si/silicide composite was measured to investigate the change in size of the silicide phase before and after the charge−discharge cycling test. The binarization process was performed on the cross-sectional SEM images of the Si/silicide composite electrode before charging and after the 50th cycle using an image-processing software (MITANI CORPORATION, Winroof) program to separate the Si phase and the silicide phase. We calculated the equivalent circle diameter by measuring the area and the number of silicide phases from the results of the image analysis. The same process was performed for five images of each sample, and we considered the average diameter of the silicide phase to be the average value.

■ ASSOCIATED CONTENT

Supporting Information

The Supporting Information is available free of charge at https://pubs.acs.org/doi/10.1021/acsomega.0c05986.

Schematic diagram of the roll-quenching method (PDF)

■ AUTHOR INFORMATION

Corresponding Author

Hiroki Sakaguchi − *Department of Chemistry and Biotechnology, Graduate School of Engineering and Center for Research on Green Sustainable Chemistry, Tottori University, Tottori 680-8552, Japan;* orcid.org/0000-0002-4125-7182; Phone: +81-857-31-5265; Email: sakaguch@chem.tottori-u.ac.jp

Authors

Yuta Kimura − *Department of Chemistry and Biotechnology, Graduate School of Engineering and Center for Research on Green Sustainable Chemistry, Tottori University, Tottori 680-8552, Japan; Daido Steel Company Ltd., Nagoya, Aichi 457-8545, Japan*

Yasuhiro Domi − *Department of Chemistry and Biotechnology, Graduate School of Engineering and Center for Research on Green Sustainable Chemistry, Tottori University, Tottori 680-8552, Japan;* orcid.org/0000-0003-3983-2202

Hiroyuki Usui − *Department of Chemistry and Biotechnology, Graduate School of Engineering and Center for Research on Green Sustainable Chemistry, Tottori University, Tottori 680-8552, Japan;* orcid.org/0000-0002-1156-0340

Complete contact information is available at: https://pubs.acs.org/10.1021/acsomega.0c05986

Author Contributions

This article was written through contributions of all the authors. All the authors have given approval to the final version of the article.

Notes

The authors declare no competing financial interest.

■ ACKNOWLEDGMENTS

The authors thank Daido Bunseki Reserch, INC. for assisting with the XRD measurement and SEM observations.

■ REFERENCES

(1) Whittingham, M. S. Lithium Batteries and Cathode Materials. *Chem. Rev.* **2004**, *104*, 4271−4302.

(2) Armand, M.; Tarascon, J.-M. Building Better Batteries. *Nature* **2008**, *451*, 652−657.

(3) Goodenough, J. B.; Kim, Y. Challenges for Rechargeable Li Batteries. *Chem. Mater.* **2010**, *22*, 587−603.

(4) Obrovac, M. N.; Krause, L. J. Reversible Cycling of Crystalline Silicon Powder. *J. Electrochem. Soc.* **2007**, *154*, A103−A108.

(5) Kim, J. W.; Ryu, J. H.; Lee, K. T.; Oh, S. M. Improvement of silicon powder negative electrodes by copper electrodes deposition for lithium secondary batteries. *J. Power Sources* **2005**, *147*, 227−233.

(6) Wang, G. X.; Sun, L.; Bradhurst, D. H.; Zhong, S.; Dou, S. X.; Liu, H. K. Nanocrystalline NiSi alloy as an anode material for lithium-ion batteries. *J. Alloys Compd.* **2005**, *306*, 249−252.

(7) Park, M.-S.; Lee, Y.-J.; Rajendran, S.; Song, M.-S.; Kim, H.-S.; Lee, J.-Y. Electrochemical properties of Si/Ni alloy-graphite composite as an anode material for Li-ion batteries. *Electrochemica Acta* **2005**, *50*, 5561−5567.

(8) Liu, W.-R.; Wu, N.-L.; Shieh, D.-T.; Wu, H.-C.; Yang, M.-H.; Korepp, C.; Besenhard, J. O.; Winter, M. Synthesis and Characterization of Nanoporous NiSi-Si Composite Anode for Lithium-Ioj Batteries. *J. Electrochem. Soc.* **2007**, *154*, A97−A102.

(9) Iida, T.; Hirono, T.; Shibamura, N.; Sakaguchi, H. Mg_2Ge/Si Composite Electrodes Prepared by Gas-Deposition as Anodes for Lithium Rechargeable Battery. *Electrochemistry* **2008**, *76*, 644−648.

(10) Sakaguchi, H.; Iida, T.; Itoh, M.; Shibamura, N.; Hirono, T. Anode Properties of LaSi2/Si Composite Thick-Film Electrodes for Lithium Secondary Batteries. *IOP Conf. Ser.: Mater. Sci. Eng.* **2009**, *1*, 012030.

(11) Usui, H.; Kashiwa, Y.; Iida, T.; Sakaguchi, H. Anode properties of Ru-coated Si thick film electrods prepared by gas-deposition. *J. Power Sources* **2010**, *195*, 3649−3654.

(12) Usui, H.; Nishinami, H.; Iida, T.; Sakaguchi, H. Anode Properties of Cu-Coated Si Thick Film Electrodes Prepared by

Electroless Deposition and Gas-Deposition. *Electrochemistry* **2010**, *78*, 329−331.
(13) Usui, H.; Shibata, M.; Nakai, K.; Sakaguchi, H. Anode properties of thick-film electrodes prepared by gas deposition of Ni-coated Si particles. *J. Power Sources* **2011**, *196*, 2143−2148.
(14) Usui, H.; Maebara, K.; Nakai, K.; Sakaguchi, H. Anode Properties of Composite Thick-Film Electrodes Consisted of Si and Various Metal Silicides. *Int. J. Electrochem. Sci.* **2011**, *6*, 2246−2254.
(15) Usui, H.; Kono, T.; Sakaguchi, H. Novel Composite Thick-Film Electrodes Consisted of Zinc Oxide and Silicon for Lithium-Ion Battery Anode. *Int. J. Electrochem. Sci.* **2012**, *7*, 4322−4334.
(16) Usui, H.; Uchida, N.; Sakaguchi, H. Improved Anode Performance of Ni-P-Coated Si Thick-Film Electrodes for Li-Ion Battery. *Electrochemistry* **2012**, *80*, 737−739.
(17) Usui, H.; Wasada, K.; Shimizu, M.; Sakaguchi, H. TiO_2/Si composites synthesized by sol-gel method and their improved electrode performance as Li-ion battery anodes. *Electrochim. Acta* **2013**, *111*, 575−580.
(18) Usui, H.; Nouno, K.; Takemoto, Y.; Nakada, K.; Ishii, A.; Sakaguchi, H. Influence of mechanical grinding on lithium insertion and extraction properties of iron silicide/silicon composites. *J. Power Sources* **2014**, *268*, 848−852.
(19) Domi, Y.; Usui, H.; Itoh, H.; Sakaguchi, H. Electrochemical lithiation and delithiation properties of ceria-coated silicon electrodes. *J. Alloys Compd.* **2017**, *695*, 2035−2039.
(20) Kimura, Y.; Domi, Y.; Usui, H.; Sakaguchi, H. Lithiation and Delithiation Properties of Silicide/Si Composite Alloy Electrodes Prepared by Rapid Quenching Method. *Electrochemistry* **2020**, *88*, 330−332.
(21) Domi, Y.; Usui, H.; Takemoto, Y.; Yamaguchi, K.; Sakaguchi, H. Improved Electrochemical Performance of Lanthanum Silicide/Silicon Composite Electrode with Nickes Substitution for Lithium-Ion Batteries. *J. Phys. Chem. C* **2016**, *120*, 16333−16339.
(22) Domi, Y.; Usui, H.; Nakabayashi, E.; Kimura, Y.; Sakaguchi, H. Effect of Element Substitution on Electrochemical Performance of Silicide/Si Composite Electrodes for Lithium-Ion Batteries. *ACS Appl. Energy Mater.* **2020**, *3*, 7438−7444.
(23) Usui, H.; Nomura, M.; Nishino, H.; Kusatsu, M.; Murota, T.; Sakaguchi, H. Gadolinium silicide/silicon composite with excellent high-rate performance as lithium-ion battery anode. *Mater. Lett.* **2014**, *130*, 61−64.
(24) Du, Z.; Ellis, S. N.; Dunlap, R. A.; Obrovac, M. N. Ni_xSi_{1-x} Alloys Prepared by Mechanical Milling as Negative Electrode Materilas for Lithium Ion Batteries. *J. Electrochem. Soc.* **2016**, *163*, A13−A18.
(25) Takeshita, K.; Shingu, P. H. An Analysis of the Ribbon Formation Process by the Single Roller Rapid Solidification Technique. *Trans. Jpn. Inst. Met.* **1983**, *24*, 529−536.
(26) Hong, S.; Xie, Z.; Dong, F.; Fei, D. Differences in microstructure and magnetic properties between directly-quenched and optimally-annealed Nd-Fe-B nanocomposite materials. *Physica B* **2010**, *405*, 690−693.
(27) Domi, Y.; Usui, H.; Shindo, Y.; Yodoya, S.; Sato, H.; Nishikawa, K.; Sakaguchi, H. Electrochemical Lithiation and Delithiation Properties of $FeSi_2$/Si Composite Electrodes in Ionic-Liquid Electrolytes. *Electrochemistry* **2020**, *88*, 548−554.

https://doi.org/10.1021/acsomega.0c05986
ACS Omega 2021, 6, 8862−8869